Open Access Journal

Journal of Power Technologies 99 (2) (2019) 58–66

journal homepage:papers.itc.pw.edu.pl

Simplified numerical model of magnetocaloric cooling device

Paweł Płuszka[a,*], Daniel Lewandowski[a], Ziemowit M. Malecha[a]

[a]*Wroclaw University of Science and Technology Wyb. Wyspianskiego 27, 50 -370 Wroclaw, Poland*

Abstract

In the present paper the laboratory scale test stand of a magnetic cooling device is briefly introduced. One set of measurements, for a given geometry of a magnetic bed filled with gadolinium, are presented and used as reference results for developing a zero-dimensional (0D) mathematical model. The 0D model assumes adiabatic heat transfer in the magnetic bed and thermal interaction of the system with surrounding ambient air. Moreover, it takes into consideration the basic dimensions of the bed geometry. Its results give a theoretical upper limit of a temperature span of the proposed magnetic cooling device. The ultimate goal of the proposed 0D numerical model is to gain insight into the basic physics needed to build a full CFD model and optimize system efficiency so as to approach the theoretical temperature limits.

Keywords: magnetic refrigeration, AMR gadolinium cycle, zero-dimensional modeling

1. Introduction

Magnetocaloric cooling can be effectively used as an alternative to a conventional compressor cooling system. The cooling capacity provided by magnetocaloric systems designed and published in recent years could find ready application in the refrigeration industry, with special interest in the home appliances branch. The attractive feature of this technology is the fact that it is environmentally safe, which is especially valuable in terms of the rapidly growth in cooling demands worldwide [1]. According to recent reports, by 2060 energy consumed for cooling will overtake that used for heating [2]. In related moves, global eco-regulations are introducing restrictions on use of HCFC gases, which are reported to have a negative effect on ozone layer depletion. As a general result of these trends, conventional vapor-compressed appliances will face increasingly rigorous legal limitations over the next couple of decades. This creates an attractive opportunity to develop alternative cooling concepts

Studies into the physics of solid materials have shown that some chemical elements and compounds change temperature when excited by external force fields. For room temperature applications it is common to treat these materials with either a magnetic or a mechanical field, which can have three main effects: magnetocaloric (driven by the magnetic field) and elasto- or barocaloric effects, caused by pressure variation on the material [3, 4] driven by either a single or three axis mechanical field [5]. We note that the combined interaction of both mechanic and magnetic fields enhances the magnitude of the temperature variation in the given material (superposition of effects). In the general case for a closed thermodynamic system, total entropy S of the material is a function of temperature T, pressure p and external magnetic field intensity H [6], as shown in the equation below:

$$S(T,p,H) = S_M(T,p,H) + S_L(T,p,H) + S_E(T,p,H) \quad (1)$$

The total entropy components are: atomic magnetic moments S_M, crystalline lattice S_L and conduction electrons S_E. In Eq. (1) the fourth component of the total entropy, atomic nucleus contribution S_N, has been deliberately omitted due to it playing an insignificant role and then only at very low, cryogenic temperatures (close to absolute zero). Consequently, it may be safely neglected for room temperature applications [6]. Since the presented work focuses solely on the magnetocaloric effect, only the magnetic-driven caloric effect is considered (no pressure effects were investigated). Another simplifying assumption is to treat the lattice and electronic parts of the entropy as temperature dependent only [6]. This approach is valid for macroscopic, engineering level evaluation. As a result, the entropy equation for magnetocaloric material is given by:

$$S(T,H) = S_M(T,H) + S_L(T) + S_E(T) \quad (2)$$

*Corresponding author

Email addresses: pawel.pluszka@pwr.edu.pl (Paweł Płuszka), daniel.lewandowski@pwr.edu.pl (Daniel Lewandowski), ziemowit.malecha@pwr.edu.pl (Ziemowit M. Malecha)

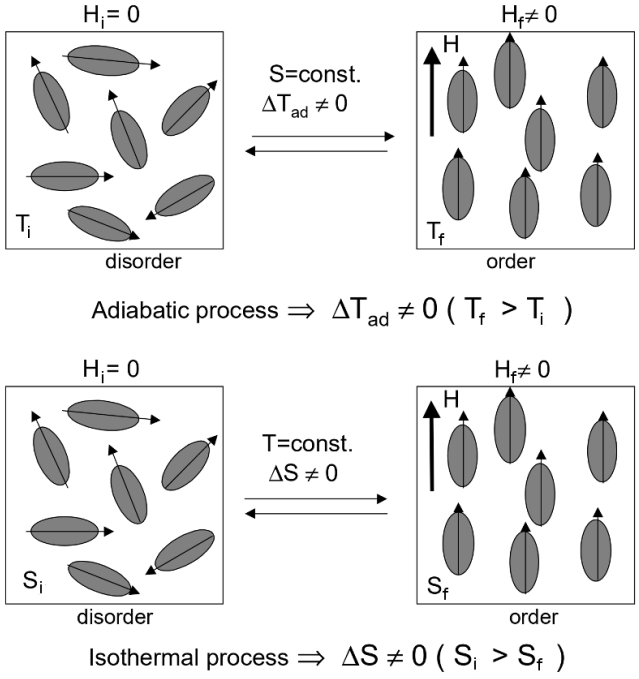

Figure 1: Scheme explaining the phenomenon of the magnetocaloric effect in both an adiabatically and an isothermally applied external magnetic field. Adapted from [7]

The magnetocaloric effect is a consequence of the coupling of magnetic moments, carried by either localized or itinerant electrons, with a variation of external magnetic field ΔH that affects magnetic entropy S_M [8]. The mechanism of MCE is discussed on Fig. 1. It is crucial to highlight that, depending on the magnetization dynamics, the MCE effect may generate different outcomes [8]:

- when the magnetic field is applied adiabatically (total entropy remains constant), the magnetic moments in the material are being ordered causing magnetic entropy to decrease; thus to sustain constant total entropy an opposite change on the sum of lattice and electronic entropy parts may be observed:

$$\begin{gathered} S(T_f, H_f) = S(T_i, H_i) \\ H_f - H_i > 0 \\ S_{M,f} - S_{M,i} < 0 \\ (S_{L,f} - S_{L,i}) + (S_{E,f} - S_{E,i}) > 0 \\ \Delta T_{ad} = T_f - T_i \end{gathered} \tag{3}$$

- when the magnetic field is applied isothermally (temperature remaining constant), the magnetic moments in the material are being ordered causing magnetic entropy to decrease; the sum of lattice and electronic entropy parts remains constant, so due to magnetic portion drop total entropy also decreases:

$$\begin{gathered} T_f = T_i \\ H_f - H_i > 0 \\ S_{M,f} - S_{M,i} < 0 \\ (S_{L,f} - S_{L,i}) + (S_{E,f} - S_{E,i}) = 0 \\ S_f = S_i - \Delta S_M \end{gathered} \tag{4}$$

Step-by-step theoretical formulation of MCE magnitude derived from fundamentals of the thermodynamics is available for further reference in the interesting and comprehensive works of de Oliveira et al. [6] and Franco et al. [9]. MCE can be related to the following measurable physical quantities [10]:

$$(\Delta S_M)_T = \mu_0 \int_{H_i}^{H_f} \left(\frac{\partial M}{\partial T}\right)_H dH \tag{5}$$

$$(\Delta T_{ad})_S = -\mu_0 \int_{H_i}^{H_f} \frac{T}{C_H} \left(\frac{\partial M}{\partial T}\right)_H dH \tag{6}$$

The magnetocaloric effect (MCE) is based on two major inputs: the magnitude of an externally created magnetic field and the ambient temperature in which the magnetization takes place [11]. It should be emphasized that the best possible performance of MCE is achieved when ferromagnetic material is magnetized close to the Curie point (specific temperature which defines the transition between the ferromagnetic and paramagnetic properties of the material, also known as first order transition).

There have been repeated investigations into magnetic cooling refrigerators. Brown [12] was the first to describe the concept of a magnetocaloric device exchanging heat with the surroundings. Since then, magnetic cooling research has related mainly to: development of new magnetocaloric materials [3, 4], novel magnetic field source arrangements [13, 14], investigation of different regenerative matrix geometries [15] and prototyping of magnetocaloric devices [8, 16]. One chemical element that is frequently used is gadolinium (Gd) - a lanthanide which has been intensively studied over the years [17–19]. Gadolinium is characterized by the Curie point of the typical ambient temperature level [17]. It can provide a relatively big temperature difference when a magnetic field is acting on it (the relation for Gd is approx. $\Delta T_{ad} \sim 2/3H$). The temperature change in general is 2.5 K per 1 T of magnetic field intensity [20] which makes gadolinium attractive for potential magnetic refrigeration applications.

Okamura et al. developed a rotary active magnetocaloric refrigerator, featuring 540 W maximum cooling power and a maximum temperature span of 21K [21]. Engelbrecht et al. [22] evaluated a rotary prototype exhibiting a no-load temperature span of over 25 K and maximum cooling power of 1010 W using gadolinium spheres. Arnold et al. [23] reported on a compact magnetocaloric refrigerator with a 33K no-load temperature span using 650 g of Gd. Jacobs et al. [24] built a rotary prototype using six layers of LaFeSiH particles, producing 3042 W of cooling power at zero temperature span and 2502 W over a span from 32 to 44 K with a COP coefficient of around 2.

The Gd is usually formed into small spherical particles or thin plates (the most common types of magnetic material

beds chosen by researchers). The main practical advantage of these shapes is their relative ease of manufacture. Nevertheless, other options, such as micro-channel matrix or packed screen bed, may be simulated and assesed theoretically [25]. Alloys of various chemical elements are also in frequent use [8]. The porous character of the bed brings the magnetocaloric material into contact with the fluid transporting the heat energy out of the system. The particles forming the porous bed have to be small in size (smallest particles are approx. 0.3-0.5 mm in diameter) to intensify the heat transfer phenomena and reduce the magnitude of the eddy electric currents generated as a result of magnetic field variations.

The main objective of the present study was to create a robust zero-dimensional (0D) methodology to create a mathematical description of heat and fluid flow phenomena present in the magnetocaloric cooling device. The main purpose of the developed model was to investigate a system used as a laboratory test stand. Based on this comparison the new proposals of system design optimization can be verified numerically and in the next step applied in the examined test stand.

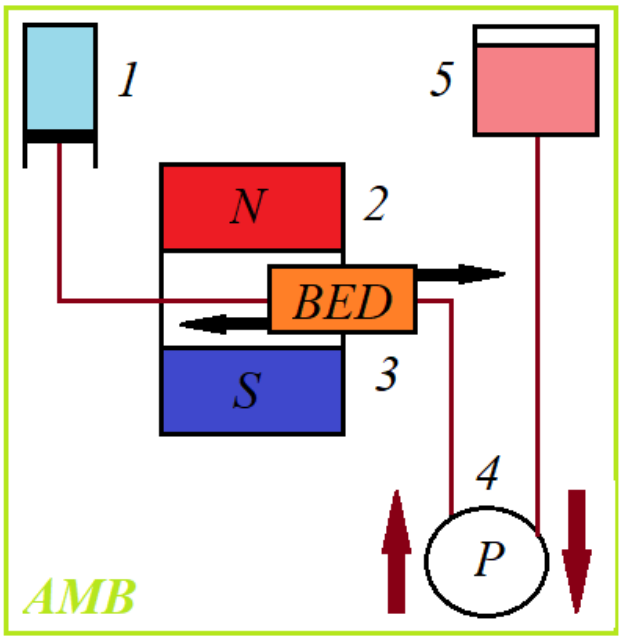

Figure 2: Schematic chart of the test stand [26]

2. Laboratory test stand

The laboratory stand used in this paper is depicted schematically on Fig. 2. For further reference see [26]. The magnetic bed (3) is mounted on rails and is periodically pushed and pulled creating a reciprocating motion between the magnetic Gd bed and the magnets. It delivers cyclical and consecutive magnetization and demagnetization states [26]. Liquid is pumped (4) two-directionally through the system, exchanging energy with the bed. Due to reciprocation cycling, generating MCE effect and two-directional pumping of liquid, the temperature (measured by thermocouples) on both the cold (1) and the hot (2) side of the system starts to diverge from the initial ambient (AMB) conditions.

The properties of the Gd material used were measured for th purpose of performing a basic assessment of system performance. Fig. 3 presents the characterization of the Gd properties obtained, influenced by the magnetic field varying in the range 0-1 T. The curves were used as input values in the 0D model described below. The temperature the Gd particles gained or lost due to two-state magnetic impact was obtained by the point-interpolation of the experimentally acquired dataset. It is observed that the specific heat and temperature rise vary the most in the range 270-300 K. In this region, the magnitude of MCE strongly depends on the ambient temperature of the system. Measurements are available up to approx. 307 K. Consequently, it is also a boundary limit for the 0D numerical model.

3. Developed 0D model

Fig. 4 conceptually presents the mathematical 0D model which was designed to reproduce the experimental setup described in [26]. The novelties of the proposed 0D model include parallel computations using multiple processors (which calculate heavy tasks in an acceptable timeframe) and incorporation of the heat loss model present in both magnetic bed and liquid tanks. In the present model, the shape of each Gd piece is assumed to be perfectly spherical. The bed is represented as a system of sequentially arranged single Gd particles. Every sphere is not in contact with its neighbors and is fully separated by a volume of liquid (called: unit flow operation). 20% ethylene glycol – water solution was considered as a liquid medium. The Gd element immersed in the volume of liquid is called a segment and is considered as a unit system in which all the physical phenomena take place. The number of segments in model is equal to the number of bed particles used in the experimentation procedure and hence is equivalent to the total bed mass. The volumes occupied in every segment by each of the phases are derived from the experiment. The segments are considered to be cylindrical. Local porosity changes are not considered in the 0D model, as porosity in each of the segments equals the overall calculated total porosity for the whole bed.

The flow is perceived as iterative propagation of a portion of liquid between each two consecutive boxes. In this conceptual approach the calculations do not include pressure or flowrate. Nonetheless, the presented method is consistent with the experiment by setting the number of liquid unit flow operations to be equivalent to the total volume of liquid pumped through the system in each cycle. A similar method was applied to model the heat transfer between the Gd solid particles and liquid passing by. In general, the heat transfer between the bed and liquid is designed as a set of equilibrium energy balances. In each segment, if a temperature

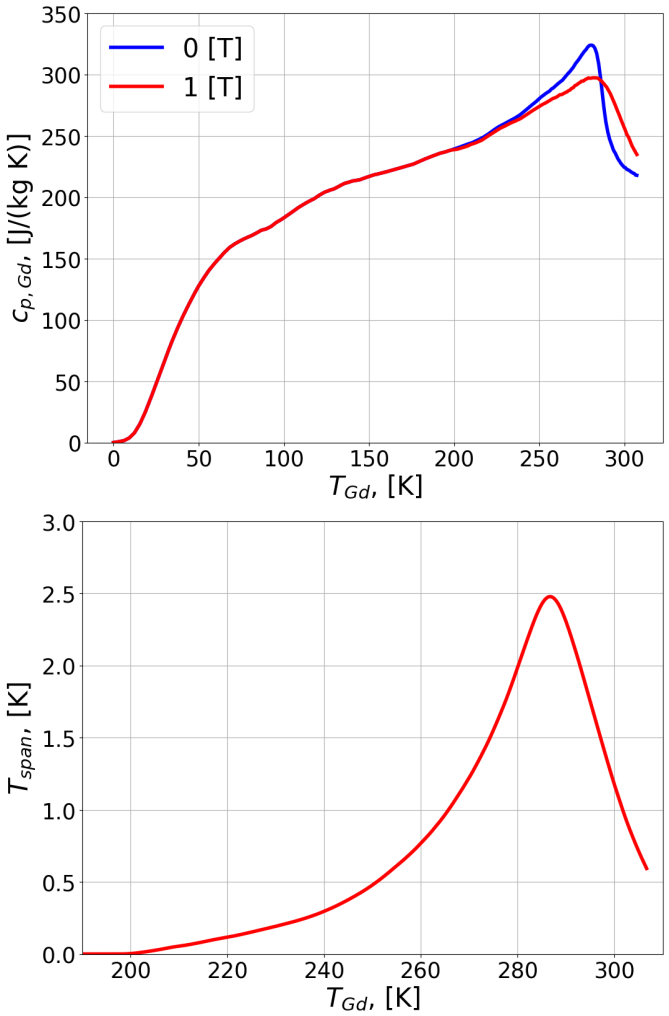

Figure 3: Experimental measurements of the Gd material used in the study. Top – specific heat capacity, bottom – temperature span. Magnetic field characterized by magnetic flux density of 1 T

difference between solid and liquid is detected, the simple equation for energy balance is applied:

$$m_{Gd}c_{p,Gd}\left(T_{end}-T_{Gd,st}\right)=m_{liq}c_{p,liq}\left(T_{end}-T_{liq,st}\right) \quad (7)$$

and the new output temperature T_{end}, identical for both phases, may be calculated. According to Fig. 3 the specific heat of Gd varies significantly in the desired range of temperatures for both magnetized and non-magnetized state. Hence, the constant $c_{p,Gd}$ value could not be employed. The solution is to interpolate the experimental curve data points (Fig. 3) and integrate them numerically over the considered temperature levels. As a consequence, Eq. (7) needs to be solved iteratively. The stop criterion was set for 0.01% of difference between each two consecutive iterations.

Additionally, a heat transfer interaction with surroundings was implemented. The free convection heat transfer coefficients was calculated from the either Churchill-Chu [27] (for cylindrical slices of bed or pipe):

$$N_D^{1/2}=0.60+0.387\left(\frac{Gr_DPr}{\left(1+(0.559/Pr)^{9/16}\right)^{16/9}}\right) \quad (8)$$

or Chu [28] (for spherical cold tank) correlations:

$$N_D=2+0.589\left(\frac{(Gr_DPr)^{1/4}}{\left(1+(0.469/Pr)^{9/16}\right)^{4/9}}\right) \quad (9)$$

Different heat transfer areas were considered for each component of the system (see Fig. 4) e.g. the sphere (for spherical cold reservoir), the side surface of the cylindrical segment (for cylindrical bed) and the side surface of the pipe slice (for linear pipe, hot reservoir). The latter case corresponds to the volume transported out of the system in single unit flow operation.

Equations responsible for the heat losses were incorporated into the existing model after the calculation step of the adiabatic energy balance. The adiabatic T_{end} temperature from Eq. (7) is treated as an input in the convective heat transfer coefficient correlation. The next step was to calculate the heat flux to be dispersed in the surroundings using all three quantities needed. The corrected temperature of the segment was used in the next iteration.

To counter overly intensive heat losses, a time constraint was introduced. It was derived based on the experimental inputs and defined as:

$$t_{loss}=\frac{t_{tot}}{n_{it}} \quad (10)$$

where t_{tot} stands for the total pumping time of the pump to transfer the whole liquid from one side of the system to the other, n_{it} is the number of liquid transport operations, as in each operation a constant liquid volume is carried. For the experimental setting used as a reference in this paper the t_{loss} value has the order of 10^{-3} s. The time constraint of heat losses, defined in Eq. (10), was introduced only in the hot and cold reservoirs. The thermal losses from the magnetic bed were described as equilibrium processes in order to maintain consistency with the aforementioned approach of modeling energy balances inside the AMR bed. In summary, the 0D model proposes an approach in which the bed is transformed into a linear, sequential arrangement of bed particles, through which a certain volume of liquid, expressed as a number of unit flow operations, is being pumped. Every unit flow operation is coupled with a respective unit thermal operation, which is assumed to be a simple equilibrium heat balance.

4. Results

A multivariate small-scale study was conducted to characterize mutual dependencies between segments and unit flow operations and the influence of hot and cold tanks (at that

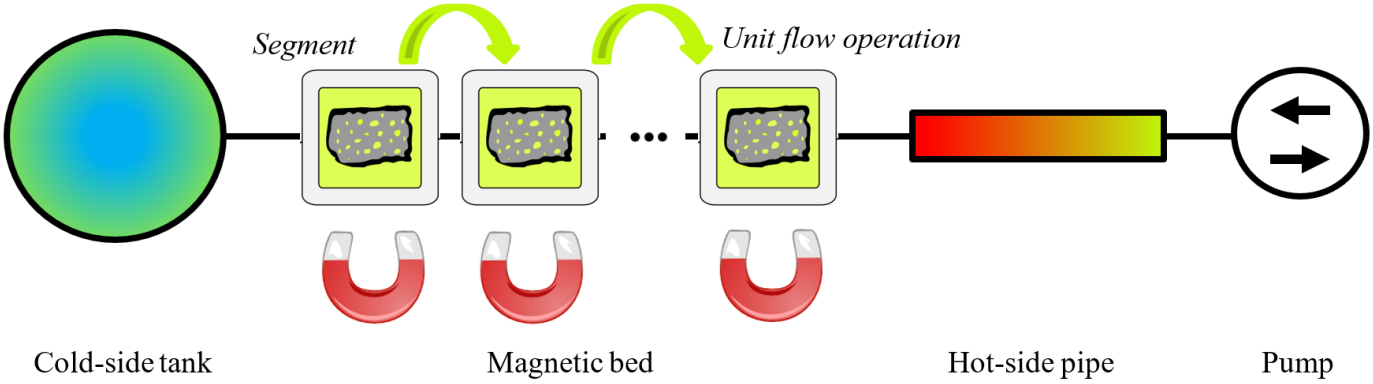

Figure 4: Final concept of the developed 0D model, used for comparison with experimental values

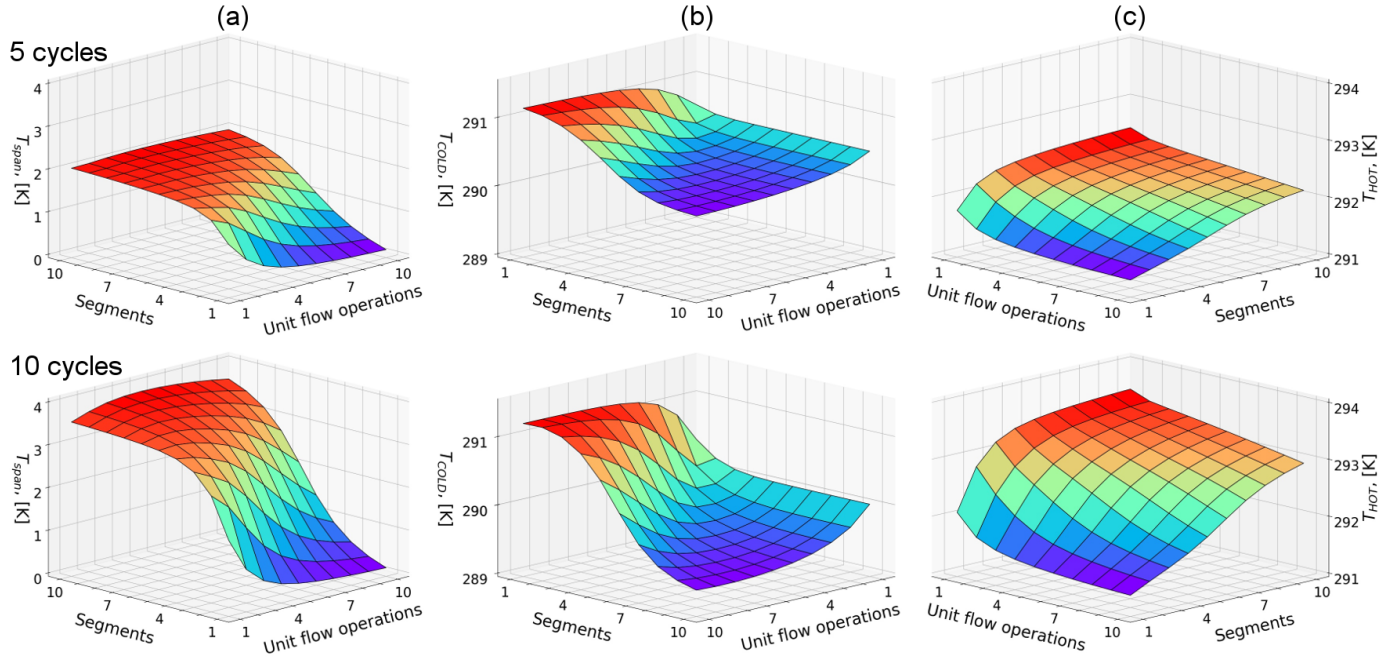

Figure 5: Temperature span (a) between cold tank temperature (b) and hot tank (c) for the system working for a duration of 5 cycles (top) and 10 cycles (bottom)

time the pipe was replaced with a spherical tank, equal in volume to the cold one). The results obtained are presented on Fig. 4. Two series of calculations were conducted for 5 and 10 cycles respectively. In all three cases an increasing number of segments contribute to better effectiveness, which is expressed by magnitudes of temperature variations.

Based on conclusions derived from the small-scale study from Fig. 4, it was decided to investigate bigger systems that are at a similar level of complexity as the experimental porous bed. The assumed number of segments represented the example bed investigated in previous works (443 Gd particles were represented by an identical number of segments). Fig. 6 presents three different values (0.25, 0.5 and 0.75 ml) of volume V_{pump} bidirectionally pumped in every cycle. The system during several dozen cycles reached very high levels of temperature span between the tanks. This behavior of the system is caused by increasing the number (frequency) of unit heat transfer events between Gd particles and liquid, indicating efficient performance. Variation of V_{pump} volume directly corresponds to the number of unit flow operations (104, 208 and 311 respectively). Therefore, for the most complicated case of 0.75 ml the number of energy balances is equal to $2 \cdot 443 \cdot 150$. Due to the adiabatic character of heat transfer unit operations, the thermal effects accumulate very fast as the consecutive cycles are pending.

The course of cold side curves indicates that the case 0.75 ml in the region of approx. the 110th cycle after gradual flattening is warmer than the temperature from the case 0.50 ml. This observation might indicate the existence of a theoretical optimum of input parameter combinations (mainly segments and unit flow operation), which can deliver the best results.

Fig. 6 indicates that without the heat loss model the hot side fluid dynamically increases the temperature, reaching a level of 310 K in approx. 150 cycles. This observation is followed by a conclusion that gadolinium particles first those located close to the hot side and eventually all of them, can reach the temperature of 307 K, which is the limiting value for the experimental gadolinium data provided for the study. As a consequence, due to the lack of experimental data, the adiabatic version of the presented 0D model cannot be applied beyond the point when the first gadolinium particle reaches the temperature of 307 K. Following the addition of the heat losses model, the calculations were repeated, but this time for inputs corresponding to the most recently performed experiment (Tab. 1). Fig. 4 presents the course of hot and cold temperatures in the simulated system. Both experiment and simulation were compared for 1000 working cycles, which is equal to the time of 1315 s. Considering the hot side, the simulation provides good agreement with the experiment. As the system is exposed to the ambient temperature, the heat losses intensify while the hot-side temperature is increases over cycles. For an ambient temperature of approx. 20℃ the losses equal the heat gains due to the adiabatic gain in the temperature of Gd particles generated by MCE. Similar behavior can be observed in the model. The fluctuations of plots are related to the relatively significant temperature gradient in the pipe, which is formed when the fluid is pumped out of the system and exposed for thermal contact with the ambient temperature.

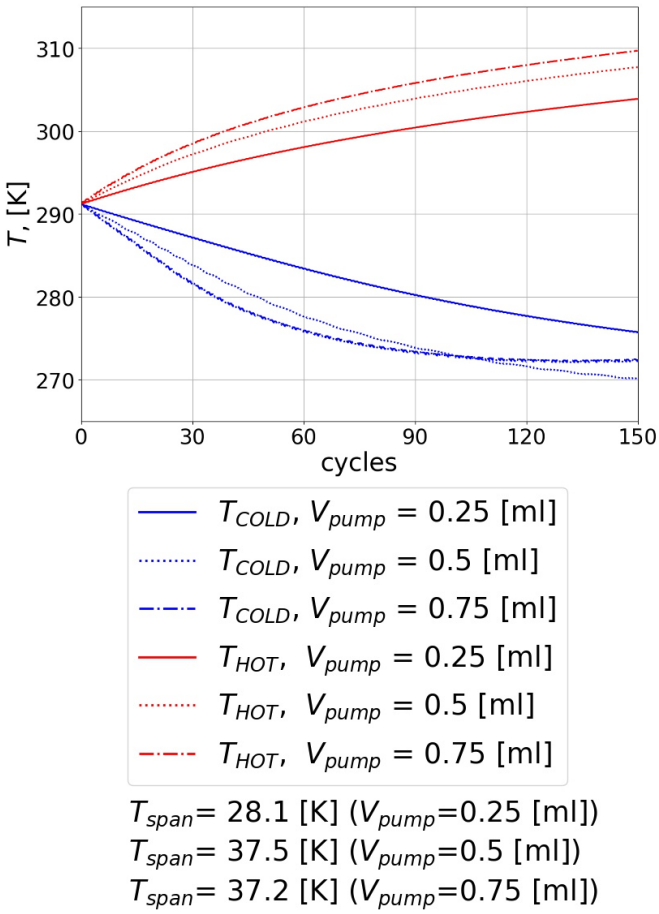

Figure 6: Adiabatic full-scale model for example experimental data. Various total volume transported through system

The cold side temperature was significantly colder in the simulation than in the experiment. Assuming best possible conditions for heat and fluid flow in the magnetic bed, it enabled the system to reach its theoretical upper limit of performance. Due to maximum effectiveness of heat removal from Gd particles generating the MCE effect, the cold side of the device reached temperatures of approx. 10 K colder than the ambient (initial) temperature. There are a few reasons for this behavior of the idealized system e.g. lack of time constraint for the heat transfer duration, perfect contact of solid gadolinium particle with a liquid and instantaneous time of magnetization and demagnetization. The temperature span, presented on Fig. 4, visualizes the difference between the effectiveness of both systems. The experimental test stand was able to achieve a span magnitude of approx. 5 K, while in the simulation the idealized model reached the three-times higher value of approx. 15 K. An optimized design of magnetic porous bed, which can provide intensified heat transfer between particles and liquid, is crucial for magnetocaloric cooling devices. The most important directions

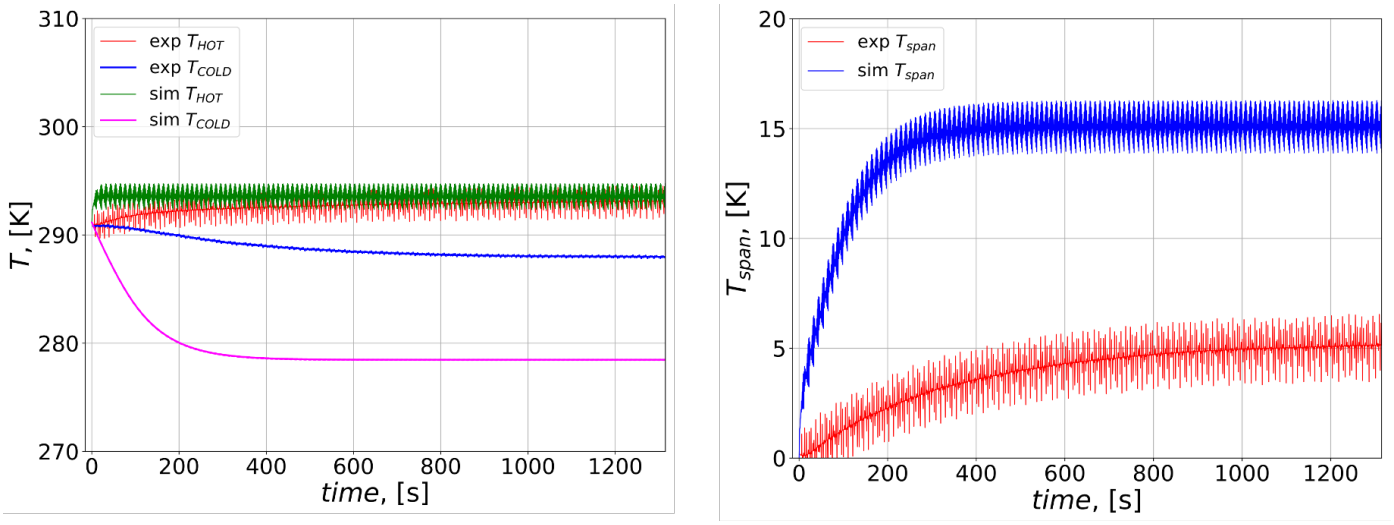

Figure 7: Experimental measurements of the Gd material used in the study. Left – specific heat capacity, right – temperature span. Magnetized by a field intensity of 1 T

Table 1: Experimental data

Quantity	Value
Total mass of Gd bed	9 g
Average diameter of single particle	1.6 mm
Bed cartridge diameter	8 mm
Bed length	43.7 mm
Cold tank volume	0.8 ml
Pumped liquid volume	0.1618 ml
Time of pumping	0.419 s
Time of magnet motion	0.179 s
Time of single cycle	1.315 s
Ambient temperature	18 C
Number of cycles	1000
Achieved temperature span	approx. 5 K

of system optimization are: finding the best porosity of the bed, decrease in bed pressure drop, study of various shapes of bed particle (spheres, plates, regular and irregular matrices), definition of the best fluid flowrate and derivation of the optimal bed length / diameter ratio. These aspects may be studied with the help of CFD numerical methods to develop an extensive directional investigation of the magnetic cooling device.

5. Conclusions

The article presents the 0D model of the magnetocaloric cooling test stand. The bed was reproduced as a sequence of Gd-liquid segments, in which flow and heat transfer phenomena were implemented. The results of the calculations confirm that the system's performance may be improved by increasing the unit heat transfer balances between the magnetocaloric material and liquid fluid. Generally, it may be achieved by increasing the total mass of the bed, having particles of a smaller diameter and increasing the fluid flowrate through the bed. The latter option may be not effective in the real device, as the pressure drop through the bed will also increase in this way. The full-scale adiabatic model showed that there is an optimal volume of fluid transported in the system.

The adiabatic approach initially used contributed to the extreme temperature span (order of tens of kelvins). The main reason for this was the lack of heat losses considerations, which increase in magnitude as the cold and hot side of system diverges across the cycles from the starting ambient conditions. A heat loss mechanism was implemented in order to model the heat transfer phenomena more coherently with the real process. Its main feature is to constrain the heat loss intensity through introducing a time limit of unit operation. It decreased the heat losses and ensured thermal behavior that was similar to the experimental measurements. The numerical simulation provided a temperature span of approx. 15 K. Compared to the experimentally achieved temperature span of approx. 5 K, it appears that the performance of the Gd bed in question can be improved. The conclusions derived with the 0D model confirm there is a performance gap between the experimental values obtained and the theoretical bound limits defined by the model. The described approach introduced several significant simplifications to the hydrodynamics and heat transfer phenomena for the porous bed flow. This provides a sound basis for developing a more detailed model based on CFD methodology. Creating a CFD model capable of capturing the necessary physics and the complexity of the considered flow will be the next step in these studies.

The general developmental trend in magnetocaloric coolers from the thermodynamic efficiency point of view should be concentrated on two key elements:

- Maximization of the temperature span between hot and cold reservoirs,
- Minimization of the cold reservoir temperature in order

to increase the cooling potential of the system.

The second point is especially important for potential magnetocooling applications in industry, due to the common requirement to maintain air temperature in home appliance freezers at -18℃ and lower. In vapor-compressed systems this condition is fulfilled by the refrigerant's evaporating temperature being 6-12 K lower than the target temperature. In a magnetocaloric cooling system, the function of the cold tank is similar to the role of the evaporator, which implies that temperature in the cold reservoir must be lower than the temperature of the freezing compartment. However, this requirement is not applicable to wine coolers, which can be satisfied with an internal compartment temperature higher than for refrigerators. Taking this fact into consideration, these appliances seem to be the first potential application of the described magnetocooling system in the home appliance industry.

Acknowledgements

The work has been supported by statutory funds from Polish Ministry for Science and Higher Education No. 0401/0168/17.

References

[1] M. Isaac, D. van Vuuren, Modeling global residential sector energy demand for heating and air conditioning in the context of climate change, Energy Policy 37 (2) (2009) 507–521.
[2] R. Teverson, T. Peters, M. Freer, J. Radcliffe, L. Koh, et al., Doing cold smarter, Tech. rep. (2015).
[3] K. Sandeman, Magnetocaloric materials: the search for new systems, Scripta Materialia 67 (6) (2012) 566–571.
[4] A. Smith, C. Bahl, R. Bjørk, K. Engelbrecht, K. Nielsen, P. N., Materials challenges for high performance magnetocaloric refrigeration devices, Advanced Energy Materials 11 (2) (2012) 1288–1318.
[5] S. Fähler, Caloric effects in ferroic materials: New concepts for cooling, Energy Technology 6 (8) (2018) 1394–1396.
[6] N. de Oliveira, P. von Ranke, Theoretical aspects of the magnetocaloric effect, Physics Reports 489 (4) (2010) 89–159.
[7] F. Casanova i Fernàndez, Magnetocaloric effect in Gd5(SixGe1-x)4 alloys, Ph.D. thesis, Universitat de Barcelona (2014).
URL http://hdl.handle.net/10803/1789
[8] V. Pecharsky, K. Gschneider Jr, Advanced magnetocaloric materials: what does the future hold?, International Journal of Refrigeration 29 (8) (2009) 1239–1249.
[9] V. Franco, J. Blázquez, J. Ipus, J. Law, L. Moreno-Ramírez, A. Conde, Magnetocaloric effect: From materials research to refrigeration devices, Progress in Materials Science 93 (2018) 112–232.
[10] A. Tishin, Y. Spichkin, The magnetocaloric effect and its applications, Materials Today 6 (11) (2003) 51.
[11] V. Pecharsky, K. Gschneider Jr, Magnetocaloric effect and magnetic refrigeration, Journal of Magnetism and Magnetic Materials 200 (1-3) (1999) 44–56.
[12] G. Brown, Magnetic heat pumping near room temperature, Journal of Applied Physics 47 (8) (1976) 3673–3680.
[13] R. Bjørk, C. Bahl, A. Smith, D. Christensen, P. N., An optimized magnet for magnetic refrigeration, Journal of Magnetism and Magnetic Materials 322 (21) (2010) 3324–3328.
[14] R. Bjørk, C. Bahl, A. Smith, P. N., Review and comparison of magnet designs for magnetic refrigeration, International Journal of Refrigeration 33 (3) (2010) 437–448.
[15] K. Engelbrecht, K. Nielsen, P. N., An experimental study of passive regenerator geometries, International Journal of Refrigeration 34 (8) (2011) 1817–1822.
[16] B. Yu, M. Liu, P. Egolf, A. Kitanovski, A review of magnetic refrigerator and heat pump prototypes built before the year 2010, International Journal of Refrigeration 13 (6) (2010) 1029–1066.
[17] S. Benford, G. Brown, Magnetic heat pumping near room temperature, Journal of Applied Physics 52 (3) (1982) 2110.
[18] B. Ponomarev, Magnetic properties of gadolinium in the region of paraprocess, Journal of Magnetism and Magnetic Materials 61 (1-2) (1986) 129–138.
[19] V. Pecharsky, K. Gschneider Jr, Magnetocaloric effect from indirect measurements: Magnetization and heat capacity, Journal of Applied Physics 86 (1) (1999) 568.
[20] Y. S. Koshkid'ko, J. Ćwik, T. Ivanova, S. Nikitin, M. Miller, K. Rogacki, Magnetocaloric properties of gd in fields up to 14 t, Journal of Magnetism and Magnetic Materials 433 (2017) 234–238.
[21] T. Okamura, Im-provement of 100 w class room temperature magnetic refrigerator, Proceedings 2nd International Confer-enee on Magnetic Refrigeration at Room Temperature, 2007 (2007) 377–382.
[22] K. Engelbrecht, D. Eriksen, C. Bahl, R. Bjørk, J. Geyti, J. Lozano, K. Nielsen, S. F., A. Smith, P. N., Experimental results for a novel rotary active magnetic regenarator, International Journal of Refrigeration 35 (6) (2012) 1498–1505.
[23] D. Arnold, A. Tura, A. Ruebsaat-Trott, A. Rowe, Design improvements of a permanent magnet active magnetic refrigerator, International Journal of Refrigeration 37 (2014) 99–105.
[24] S. Jacobs, J. Auringer, A. Boeder, J. Chell, L. Komorowski, J. Leonard, S. Russek, C. Zimm, The performance of a large-scale rotary magnetic refrigerator, International journal of refrigeration 37 (2014) 84–91.
[25] T. Lei, K. Engelbrecht, K. Nielsen, C. Veje, Study of geometries of active magnetic regenerators for room temperature magnetocaloric refrigeration, Applied Thermal Engineering 111 (2017) 1232–1243.
[26] A. Czernuszewicz, J. Kaleta, D. Kołosowski, D. Lewandowski, Experimental study of the effect of regenerator bed length on the performance of a magnetic cooling system, International Journal of Refrigeration 97 (2019) 49–55.
[27] S. Churchill, H. Chu, Correlating equations for laminar and turbulent free convection from vertical plates, International Journal of Heat and Mass Transfer 18 (11) (1975) 1323–1329.
[28] S. Churchill, Laminar free convection from a horizontal cylinder with a uniform heat flux density, Letters in Heat and Mass Transfer 2 (1) (1974) 109–111.

Nomenclature

Letters

c_p	specific heat, J/(kg·K)
ΔS_M	isothermal MCE magnetic entropy change, J/K
t	time, s
T	temperature, K
V	volume, ml
ΔT_{ad}	adiabatic MCE temperature change, K
μ_0	agnetic permeability of space (vacuum), H/m
C_H	heat capacity taken at constant magnetic field, J/(kg·K)
Gr_D	Grashof number
H	magnetic field strength, A/m
m	mass, kg

n_{it} number of iterations

N_D Nusselt number,

p pressure, Pa

Pr Prandtl number,

S entropy, J/K

Indexes

end end of heat balance

N nucleus

$pump$ pump

st start of heat balance

tot total

E electronic

f final

Gd gadolinium

i initial

liq liquid

$loss$ loss

L lattice

M magnetic